PAPER

Local temperature reduction induced crystallization of MASnI₃ and achieving a direct wafer production†

Zhun Yao,[a] Zhou Yang,*[a] Yucheng Liu,[a] Wangen Zhao,[a] Xiaorong Zhang,[a] Bin Liu,[a] Huan Wu[a] and Shengzhong (Frank) Liu ![ID]*[ab]

Despite the rapid advancement of perovskite solar cells, the fundamental drawback of toxicity in lead based materials has largely limited their large-scale development and application. Hence, we developed a local temperature reduction induced crystallization (LTRIC) method to directly obtain a lead-free perovskite wafer (CH₃NH₃SnI₃), which is 110 μm-thick, in an oil bath. The XRD diffraction peaks of the MASnI₃ wafer are indexed to (001) and its parallel crystal planes, demonstrating its high orientation. The UV-vis-NIR discloses that the absorption onset of the MASnI₃ wafer is red-shifted to 1015 nm, corresponding to a narrow bandgap of 1.21 eV.

Introduction

Lead halide based perovskite materials have attracted tremendous attention during the past few years because of their superior optoelectronic properties such as long carrier lifetime, high carrier mobility, long carrier diffusion length, high defect tolerance, *etc.*[1–12] Even with a lot of grain boundaries existing in the microcrystalline perovskite films, there have been several kinds of high performance optoelectronic devices developed, such as solar cells,[13–15] LEDs,[16] lasers,[17] and photodetectors.[18,19] In particular, the efficiency of the perovskite based solar cells has been increased to as high as 22.1%, approaching that of the high efficiency of crystalline silicon based solar cells.[20–22]

To further improve performance for the optoelectronic devices, it is necessary to study defect-free single-crystalline perovskite materials.[23] Single crystalline perovskite with fewer defects is the best candidate to study its intrinsic properties. Huang developed a top seed solution growth method to produce single-crystalline CH₃NH₃PbI₃ with ultra-low trap state density (3.6×10 cm^{-3}) and ultra-long carrier life time (~90 μs) and diffusion length (>175 μm).[4] Much more intriguingly, the absorption onset extended to 850 nm, around 50 nm red-shift compared to the microcrystalline films, which is better for sunlight utilization. Bakr developed an anti-solvent vapor-

assisted crystallization to prepare high quality single-crystalline CH₃NH₃PbBr₃ and CH₃NH₃PbI₃, showing similar trap density as the Huang group reported.[24] However, the carrier mobility and carrier lifetime were much smaller. Furthermore, the Bakr and Liu independently developed a high temperature induced crystallization method to produce high quality single-crystalline perovskites at high growth rate.[25,26] Even though high performance photodetectors were designed and fabricated, it appears to be challenging to fabricate high efficient single-crystalline perovskite solar cells. The Bakr group used ultrasonic triggered crystallization to adjust the crystal growth process of CH₃NH₃PbBr₃ and obtained thickness controllable single-crystalline perovskite films.[27] As reported in this intriguing work, the thickness plays an important role in determining the PCEs of single-crystalline perovskite solar cells. It is predicted that only <10 μm is needed to achieve a good photovoltaic performance. The PCE of single-crystalline perovskite solar cell will decrease dramatically as the film thickness exceed 10 μm. Wafer perovskite materials were needed while most of studies to date have been limited to bulk crystals which are difficult to be implemented for optoelectronic devices.

Herein, we report development of local temperature reduction induced crystallization (LTRIC) to prepare MASnI₃ wafer. The XRD results show the obtained wafer is well crystallized and shows strong orientation along [001]. MASnI₃ wafer shows an extended absorption spectrum with absorption onset reaching as long as 1015 nm, exceed 150 nm longer than 850 nm of the MAPbI₃ single crystal. Photoluminance (PL) peak is also red-shifted by 160 nm to 930 nm compared to MAPbI₃. The great crystallinity and optical properties make the obtained wafer a good candidate to disclose its potential in optoelectronic devices.

[a] Key Laboratory of Applied Surface and Colloid Chemistry, National Ministry of Education, Shaanxi Engineering Lab for Advanced Energy Technology, School of Materials Science and Engineering, Shaanxi Normal University, Xi'an 710062, China. E-mail: zyang@snnu.edu.cn

[b] Dalian National Laboratory for Clean Energy, iChEM, Dalian Institute of Chemical Physics, Chinese Academy of Sciences, Dalian, 116023, China. E-mail: szliu@dicp.ac.cn

† Electronic supplementary information (ESI) available. See DOI: 10.1039/c7ra07101a

Results and discussion

Fig. 1 shows photograph of the experimental setup and a 1 cm-sized MASnI$_3$ wafer prepared using LTRIC method. Thin MASnI$_3$ wafer could be found at the bottom of the precursor solution, as shown in Fig. 1a. The shape of the wafer looks like an imperfect hexagonal (Fig. 1b) that is common for general MAPbI$_3$/MASnI$_3$ perovskite crystals.[26,28] More pictures of the MASnI$_3$ wafers are provided in Fig. S1.†

The crystallinity of the obtained MASnI$_3$ wafer is examined using XRD. Fig. 2a shows the XRD result taken on an as-grown wafer. It is surprising to see that essentially only four diffraction peaks indexed to (001), (002), (003) and (004) crystal planes, are observed. All of the four peaks are originated from (001) and its parallel planes, indicating that the wafer is highly oriented along [001] direction. To confirm that there is no impurity phases in the wafer, XRD measurement was taken after the wafer is grounded into fine powder. There are many more additional peaks shown in Fig. 2b, all of which can be assigned to MASnI$_3$, which agree well with the reported data (add a citation about the XRD results). Diffraction peaks from other impurity phases are not observed.

The thickness of wafer is 110 μm deduced from the cross-sectional view of wafers (seen in Fig. 3a). There are some attachments on it as shown in Fig. 3b, which makes the surface rough. That should be the reason that the wafer looks dark rather than shiny as shown in Fig. 1b.

To find out the growth mechanism, a time dependent crystal growth process has been investigated and shown in Fig. 4a–d. As shown in Fig. 4b, small dark particle would firstly form on the surface of the precursor solution and would continue
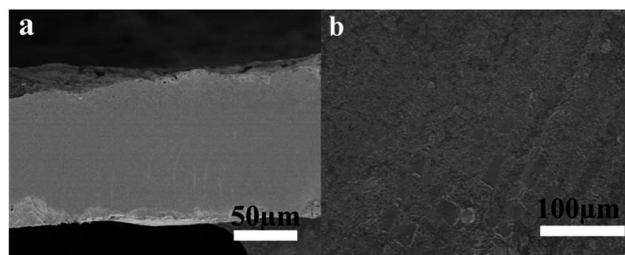

Fig. 1 Photograph of MASnI$_3$ wafers in precursor solution (a) and the as-grown MASnI$_3$ wafer (b).

Fig. 2 X-ray diffraction of (a) the MASnI$_3$ wafer and (b) MASnI$_3$ powder grounded from a wafer.

Fig. 3 The cross-sectional view (a) and surface view (b) of a MASnI$_3$ wafer.

growing to be a large wafer (Fig. 4c). Finally, the wafer will sink into the bulk solution because of its larger gravity than the buoyancy supported by the solvent. Then, new seed crystal will form and the wafer growth process will repeat. After carefully observing the wafer growth process, we found that small water drops condensed on the cork, which should be cooler than bulk solution, would fall off the cork and dive into the solution. The local temperature of the spot into which the drop dived is reduced. Due to the normal temperature dependent solubility of MASnI$_3$, lowering the solution temperature will make MASnI$_3$ solution super saturation and induce the crystallization of MASnI$_3$. The cooled spot as we mentioned should induce the formation of MASnI$_3$ crystal seed as observed in Fig. 4b. Based on the observation and the solubility property of MASnI$_3$, a LTRIC process has been proposed to interpret the formation of MASnI$_3$ wafer, as shown in Fig. 4e–i. Due to the high solvent temperature, water would evaporate quickly to form hot vapor. As the hot vapor encountered with cold cork, it would condense to a small water drop. When the water drop became larger enough, it fell off the cold cork and dropped onto the hot solution surface (Fig. 4e). The local temperature of the spot where the drop fell onto would be reduced. And the reduction in temperature could generate a driving force for perovskite crystallization because of the normal temperature dependent solubility of MASnI$_3$. Then, small crystalline seed would be formed on the surface (Fig. 4g) as we observed during the wafer growth (Fig. 4b). Further increasing the reaction time, small seed will grow to a larger wafer, which would be sink into bulk solution as it is too heavy (Fig. 4h–j).

To further verify our hypothesis, anhydrous diethyl ether induced crystallization of MASnI$_3$ has been conducted as shown in Fig. S4.† First, two precursor solutions were prepared identically and immersed in 100 °C oil bath, as shown in Fig. S4a.† And the right one was used as a reference. An anhydrous diethyl ether drop was dripped into the left solution. As anhydrous diethyl ether cannot mix well with water, anhydrous diethyl ether will evaporate quickly as it contacted hot solvent surface due to its low evaporation temperature. During the evaporation, the local temperature should be reduced as evaporation process will carry energy away. Suddenly, a lot of smaller crystals were formed on the surface (Fig. S4b†). However, there is no any sign of crystal at the surface of reference solution (on the right). As the reaction process extended, a lot of wafers were formed on the surface of the solution, as shown in Fig. S4c.† At the same
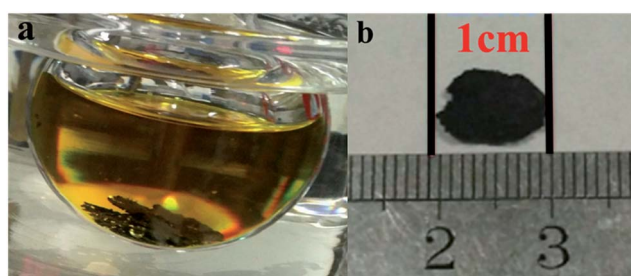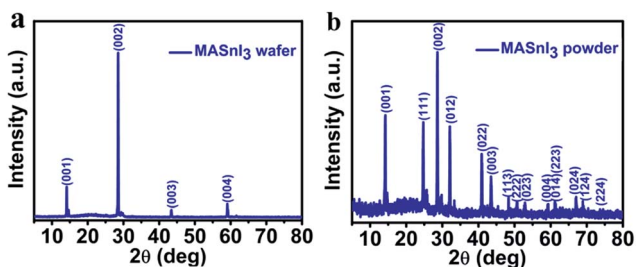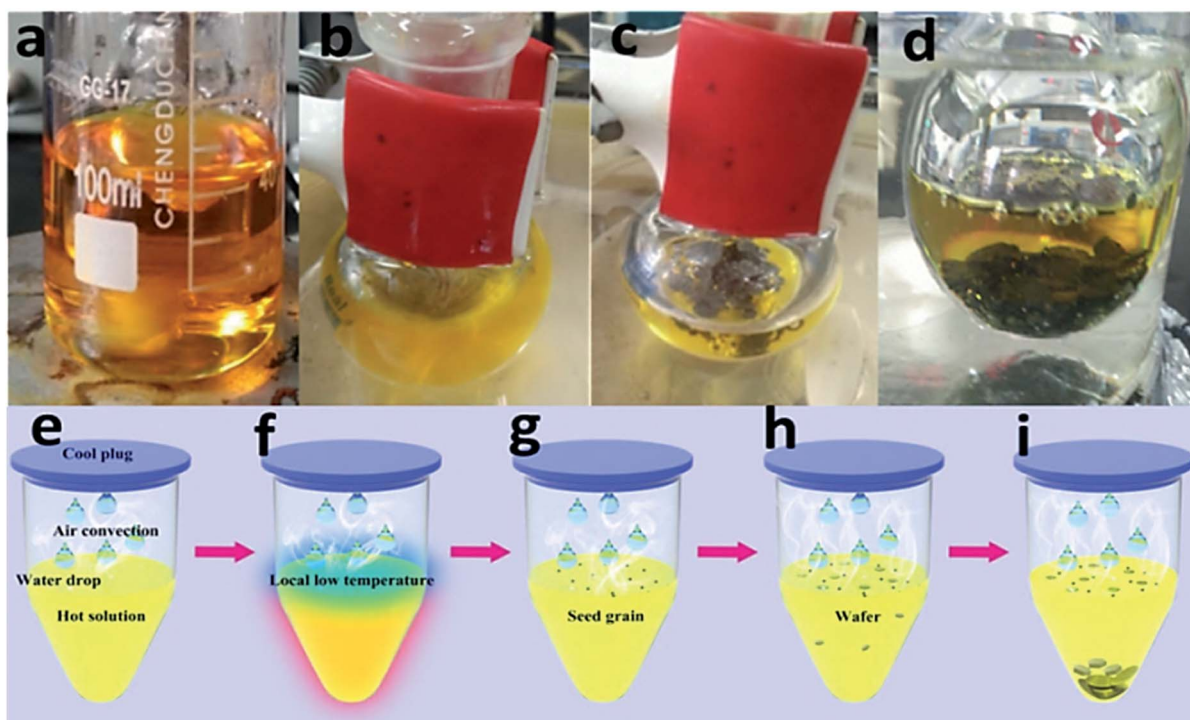
Fig. 4 Time dependent wafer process growth (a–d) and schematic illustration of the proposed LTRIC process (e–i).

time, just few small crystal seeds formed at the surface of the reference solution (Fig. S4c†). That means the quick evaporation of diethyl ether anhydrous drop accelerates the crystallization of MASnI$_3$, faster than the reference one. On the other hand, as the water on cork droplet does not easily fall off in the reference system, slower crystal formation and fewer seed crystal observed in Fig. S4c† are reasonable. Those results could be a direct prevents of our proposed LTRIC process. Cool water drop induced crystallization of MASnI$_3$ has also been done. Shiny MASnI$_3$ wafer can also be produced with good crystallinity, high orientation as well as much smoother surface as shown in Fig. S2 and S3.† Both of those model experiments demonstrate the local temperature reduction could be an effective way to trigger crystallization and induce direct wafer production.

The optical properties of the as grown crystals were investigated using UV-vis-NIR spectrum meter. Fig. 5a shows the UV-vis-NIR absorption spectra of the MASnI$_3$ perovskite, whose absorption onset located at 1015 nm. UV-vis-NIR absorption spectrum of MASnI$_3$ wafer fabricated by cool water induced crystallization is showing in Fig. S5,† which present a similar light absorption curve. The MASnI$_3$ shows strong absorption across the entire visible spectrum and therefore it is seen as black in color. The band gap value was estimated on the basis of the Tauc plot as the intercept value of the plot of $(\alpha h\nu)^{1/m}$ or $(F(R\infty)h\nu)^{1/m}$ against photon energy $h\nu$. As MASnI$_3$ is a direct-band gap semiconductor material, the m value is 1/2.[29] By extrapolating the linear region of the $(F(R\infty)h\nu)^2$ [30] to the energy-axis $h\nu$ intercept as shown in the inset, E_g of the obtained MASnI$_3$ can be established to be 1.21 eV, similar with the former reported value.[28] The obtained MASnI$_3$ exhibits PL peak at 930 nm as shown in Fig. 5b. It is interesting to see that the PL peak value is smaller than the absorption onsets, implying that the lights of PL due to the excitation can be extinguished by themselves. There is no doubt that it is advantageous for them to be applied in solar cells.[26] Considering no PL emission being observed from solution-grown MASnI$_3$ wafer material determination at room temperature, the PL appears to be much more prominent in the present wafer samples.

To examine the thermal stability of the perovskite MASnI$_3$ wafer, thermogravimetric analysis (TGA) was carried out under nitrogen flow from room temperature to 570 °C with a rate of 5 °C min^{-1}. As shown in the TGA curve (Fig. 6), the decomposition of MASnI$_3$ could be classified to two steps, corresponding to 28% weight loss between 250 °C to 323 °C, corresponding to the CH$_3$NH$_3$I evaporation. 72% weight loss between 324 °C to 538 °C. The TGA result indicates the obtained MASnI$_3$ has higher thermal stability than MAPbI$_3$ crystal, which will be thermally decomposed at 240 °C.
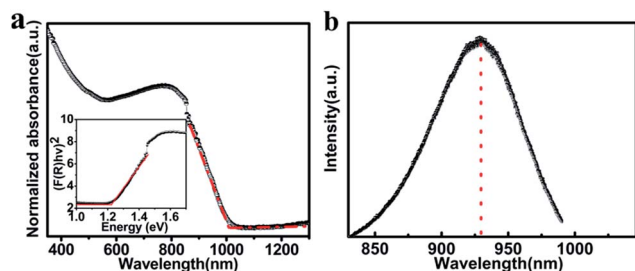

Fig. 5 UV-vis-NIR absorption spectrum, bandgap and PL spectra of MASnI$_3$ wafer.
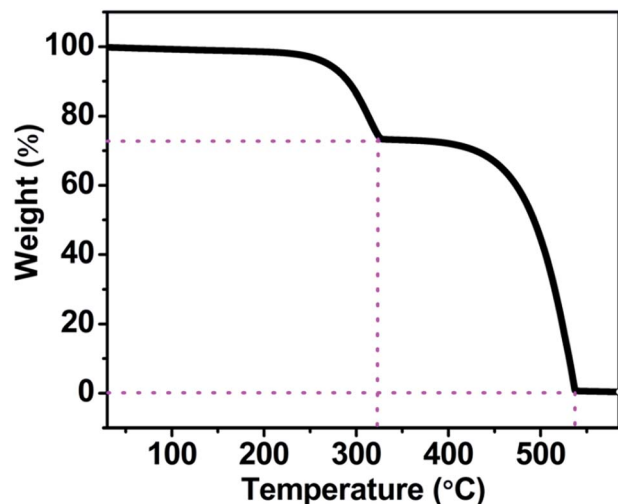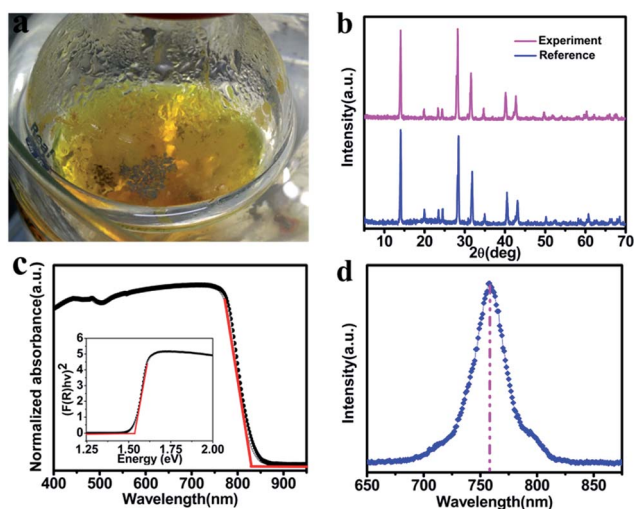
Fig. 6 Thermal gravimetric (TGA) data for MASnI$_3$ wafer.

Fig. 7 The photo, X-ray diffraction, UV-vis-NIR absorption spectrum, bandgap and PL spectra of MAPbI$_3$ wafer.

Furthermore, MAPbI$_3$ wafer has also been produced by using LTRIC method as shown in Fig. 7a. A few of MAPbI$_3$ are floating at the surface of the solution. The XRD result of the obtained wafer is same to our previously reported results,[26] demonstrating the obtained wafers are MAPbI$_3$. Its optical absorption and emission properties were also investigated as shown in Fig. 7c and d. The wafers show strong light absorption across the whole UV-Vis-NIR region with a sharp cut-off around 830 nm and photoemission peak at 760 nm, which are similar with the reported data.

Experimental

Materials

Methylamine (CH$_3$NH$_2$) (40 wt% in water), hydroiodic acid (HI) (57 wt% in water, stable with 1.5 wt% hypophosphorous), and other basic materials were purchased from Sinopharm

Chemical Reagent Ltd., China. PbAc$_2$ was purchased from Xi'an Polymer Light Technology Corp. All these materials were used as received without further purification.

Wafer preparation

MASnI$_3$ wafer preparation. CH$_3$NH$_3$I (MAI) was synthesized by reaction of hydroiodic acid and methylamine with molar ratio of 1 : 1.2, as reported in literature.[26] Fresh synthesized MAI (2.3850 g, 0.015 mol) and SnO (2.02 g, 0.015 mol) were dissolved in a mixed solvent of HI (30 mL) and H$_3$PO$_2$ (15 mL) at 80 °C. To form a transparent yellow precursor solution, the mixture was actively stirred for 8 hours. It was then transferred into a round bottom flask and submerged into an oil bath set at 100 °C. To prevent solvent evaporation, the round-bottom flask was covered with a cork. The temperature of the oil bath was slowly reduced to 98 °C in 12 h. During this process, a few small crystalline seeds were formed at the surface of the solution. As the reaction time was extended, the small seed crystals grew into larger wafers. Finally, the wafer would sink into the solution as it became bigger.

MAPbI$_3$ wafer preparation. Fresh synthesized MAI (1.59 g, 0.01 mol) and PbAc$_2$ (2.61 g, 0.01 mol) were dissolved in a mixed solvent of HI (30 mL) and H$_3$PO$_2$ (15 mL) at 70 °C. To form a transparent yellow precursor solution, the mixture was actively stirred for 8 hours. It was then transferred into a round bottom flask and submerged into an oil bath set at 70 °C. To prevent solvent evaporation, the round-bottom flask was covered with a cork. The temperature of the oil bath was slowly reduced to 60 °C in 12 h. Then a drop of diethyl ether was added onto the precursor surface to induce the crystallization. As the reaction time was extended, the small seed crystals grew into larger wafers.

Characterization

Powder X-ray diffraction (XRD) was recorded using a DX-2700 X-ray diffract meter operated at 40 kV and 30 mA. UV-Vis-NIR diffuse reflectance spectrum was measured at room temperature using an UV-Vis-NIR spectrometer (PerkinElmer Lambda 950) with an integrating sphere attachment. A highly refined barium sulfate (BaSO$_4$) powder plate was used as the reference (100% reflectance). The obtained reflectance data were used to estimate the band gap of the wafer by using the Kubelka–Munk equation: $\alpha/S = (1 - R)^2/(2R)$, where α is the absorption coefficient, S the scattering coefficient, and R the reflectance.[31] PL measurement was performed on a Renishaw in *via* Raman microscope with a 532 nm laser as excitation source. A field emission scanning electron microscopy (FE-SEM, SU-8020, Hitachi) was used to investigate the surface morphology, cross-section of the obtained wafer.

Conclusions

In summary, we had successfully and directly obtained 110 μm-thick MASnI$_3$ wafer under an ambient atmosphere by LTRIC method. After primary characterizations, it has been found that the obtained MASnI$_3$ wafer shows good crystallinity and great

orientation as well as gives a band gap of 1.21 eV, which is narrower than their corresponding thin-film material. After carefully observation and dedicated experiment design, local spot temperature reduction induced crystallization (LTRIC) has been proposed and further verified by the cold water and quick evaporation of diethyl ether anhydrous induced crystallization experiment. At the same time, $MAPbI_3$ wafer has been successfully prepared by using this method. Our technique may provide an effective strategy for growing wafer for demanding high quality, low cost device applications. Further controlling the number of crystal seed and getting rid of surface attachment should be effective ways control the crystallization and quality of $MASnI_3$ wafer.

Acknowledgements

Notes and references

1 D. T. Moore, H. Sai, K. W. Tan, D. M. Smilgies, W. Zhang, H. J. Snaith, U. Wiesner and L. A. Estroff, *J. Am. Chem. Soc.*, 2015, **137**, 2350–2358.

2 M. D. McGehee, *Nature*, 2013, **501**, 323–325.

3 H. S. Kim, C. R. Lee, J. H. Im, K. B. Lee, T. Moehl, A. Marchioro, S. J. Moon, R. Humphry-Baker, J. H. Yum, J. E. Moser, M. Gratzel and N. G. Park, *Sci. Rep.*, 2012, **2**, 591.

4 Q. Dong, Y. Fang, Y. Shao, P. Mulligan, J. Qiu, L. Cao and J. Huang, *Science*, 2015, **347**, 967–970.

5 D. Yang, R. Yang, J. Zhang, Z. Yang, S. Liu and C. Li, *Energy Environ. Sci.*, 2015, **8**, 3208–3214.

6 X. Ren, Z. Yang, D. Yang, X. Zhang, D. Cui, Y. Liu, Q. Wei, H. Fan and S. F. Liu, *Nanoscale*, 2016, **8**, 3816–3822.

7 Y. J. Fang, Q. F. Dong, Y. C. Shao, Y. B. Yuan and J. S. Huang, *Nat. Photonics*, 2015, **9**, 679–686.

8 J. Lee, H. F. Chen, T. Batagoda, C. Coburn, P. I. Djurovich, M. E. Thompson and S. R. Forrest, *Nat. Mater.*, 2016, **15**, 92–98.

9 Z. Lian, Q. Yan, Q. Lv, Y. Wang, L. Liu, L. Zhang, S. Pan, Q. Li, L. Wang and J. L. Sun, *Sci. Rep.*, 2015, **5**, 16563.

10 D. H. Cao, C. C. Stoumpos, O. K. Farha, J. T. Hupp and M. G. Kanatzidis, *J. Am. Chem. Soc.*, 2015, **137**, 7843–7850.

11 D. P. McMeekin, G. Sadoughi, W. Rehman, G. E. Eperon, M. Saliba, M. T. Horantner, A. Haghighirad, N. Sakai, L. Korte, B. Rech, M. B. Johnston, L. M. Herz and H. J. Snaith, *Science*, 2016, **351**, 151–155.

12 M. R. Filip, S. Hillman, A. A. Haghighirad, H. J. Snaith and F. Giustino, *J. Phys. Chem. Lett.*, 2016, **7**, 2579–2585.

13 M. Ibrahim Dar, M. Abdi-Jalebi, N. Arora, T. Moehl, M. Gratzel and M. K. Nazeeruddin, *Adv. Mater.*, 2015, **27**, 7221–7228.

14 D. Liu, J. Yang and T. L. Kelly, *J. Am. Chem. Soc.*, 2014, **136**, 17116–17122.

15 J. Xu, A. Buin, A. H. Ip, W. Li, O. Voznyy, R. Comin, M. Yuan, S. Jeon, Z. Ning, J. J. McDowell, P. Kanjanaboos, J. P. Sun, X. Lan, L. N. Quan, D. H. Kim, I. G. Hill, P. Maksymovych and E. H. Sargent, *Nat. Commun.*, 2015, **6**, 7081.

16 G. Wang, D. Li, H. C. Cheng, Y. Li, C. Y. Chen, A. Yin, Z. Zhao, Z. Lin, H. Wu, Q. He, M. Ding, Y. Liu, Y. Huang and X. Duan, *Sci. Adv.*, 2015, **1**, e1500613.

17 H. Zhu, Y. Fu, F. Meng, X. Wu, Z. Gong, Q. Ding, M. V. Gustafsson, M. T. Trinh, S. Jin and X. Y. Zhu, *Nat. Mater.*, 2015, **14**, 636–642.

18 B. R. Sutherland, A. K. Johnston, A. H. Ip, J. X. Xu, V. Adinolfi, P. Kanjanaboos and E. H. Sargent, *ACS Photonics*, 2015, **2**, 1117–1123.

19 G. Maculan, A. D. Sheikh, A. L. Abdelhady, M. I. Saidaminov, M. A. Haque, B. Murali, E. Alarousu, O. F. Mohammed, T. Wu and O. M. Bakr, *J. Phys. Chem. Lett.*, 2015, **6**, 3781–3786.

20 W. S. Yang, B. W. Park, E. H. Jung, N. J. Jeon, Y. C. Kim, D. U. Lee, S. S. Shin, J. Seo, E. K. Kim, J. H. Nohand and S. I. Seok, *Science*, 2017, **356**, 1376–1379.

21 V. Adinolfi, O. Ouellette, M. I. Saidaminov, G. Walters, A. L. Abdelhady, O. M. Bakr and E. H. Sargent, *Adv. Mater.*, 2016, **28**, 7264–7268.

22 J. Zhang, M.-h. Shang, P. Wang, X. Huang, J. Xu, Z. Hu, Y. Zhu and L. Han, *ACS Energy Lett.*, 2016, **1**, 535–541.

23 E. Edri, S. Kirmayer, M. Kulbak, G. Hodes and D. Cahen, *J. Phys. Chem. Lett.*, 2014, **5**, 429–433.

24 D. Shi, V. Adinolfi, R. Comin, M. Yuan, E. Alarousu, A. Buin, Y. Chen, S. Hoogland, A. Rothenberger, K. Katsiev, Y. Losovyj, X. Zhang, P. A. Dowben, O. F. Mohammed, E. H. Sargent and O. M. Bakr, *Science*, 2015, **347**, 519–522.

25 M. I. Saidaminov, A. L. Abdelhady, B. Murali, E. Alarousu, V. M. Burlakov, W. Peng, I. Dursun, L. Wang, Y. He, G. Maculan, A. Goriely, T. Wu, O. F. Mohammed and O. M. Bakr, *Nat. Commun.*, 2015, **6**, 7586.

26 Y. Liu, Z. Yang, D. Cui, X. Ren, J. Sun, X. Liu, J. Zhang, Q. Wei, H. Fan, F. Yu, X. Zhang, C. Zhao and S. F. Liu, *Adv. Mater.*, 2015, **27**, 5176–5183.

27 W. Peng, L. Wang, B. Murali, K. T. Ho, A. Bera, N. Cho, C. F. Kang, V. M. Burlakov, J. Pan, L. Sinatra, C. Ma, W. Xu, D. Shi, E. Alarousu, A. Goriely, J. H. He, O. F. Mohammed, T. Wu and O. M. Bakr, *Adv. Mater.*, 2016, **28**, 3383–3390.

28 Y. Dang, Y. Zhou, X. Liu, D. Ju, S. Xia, H. Xia and X. Tao, *Angew. Chem.*, 2016, **55**, 3447–3450.

29 S. Tsunekawa, T. Fukuda and A. Kasuya, *J. Appl. Phys.*, 2000, **87**, 1318.

30 L. Dimesso, M. Dimamay, M. Hamburger and W. Jaegermann, *Chem. Mater.*, 2014, **26**, 6762–6770.

31 F. Hao, C. C. Stoumpos, P. Guo, N. Zhou, T. J. Marks, R. P. Chang and M. G. Kanatzidis, *J. Am. Chem. Soc.*, 2015, **137**, 11445–11452.